Combined effect of fibers and steel rebars in high performance concrete

Yang Yuguang, Joost C. Walraven, Joop A. den Uijl
Delft University of Technology, the Netherlands

In this paper a brief overview on the effect of tension stiffening in normal strength concrete and High Performance Fiber Concrete (HPFC) is given. On the basis of an existing model, several simplifications are proposed to describe the post-cracking performance of HPFC, and a simplified model for practical application is developed. This model is validated using the results of a number of concentric tensile tests on prismatic reinforced HPFC elements. The results clearly show that the simplifications proposed in this paper offer sufficient accuracy in predicting the behavior of HPFC elements reinforced with conventional reinforcement.

Key words: tension stiffening, crack width, reinforced concrete

1 Introduction

In the last few years, several types of High Performance Concrete (HPFC) and Ultra High Performance Concrete (UHPFC) have been developed. By minimizing their porosity on the basis of optimizing the particle packing density in combination with the use of super-plasticizers for optimum workability, a compressive strength of more than 150 MPa can be reached. In order to reduce the brittleness of these high strength concretes, fibers are added to the mixture. This results in a more ductile performance in both compression and tension. An ultimate strain of more than 5% can be reached before the strain localizes in one crack.

Combining in one concrete steel fibres and traditional steel rebars is a good option. On the one hand, the reinforcing bars take care of the main bearing capacity of the structural member in bending. On the other hand, the steel fibres allow the design of very thin members, while they give the concrete a reliable post-peak tensile strength and ductility, making sure that the member can easily cope with the effects of splitting and spalling , occurring e.g. in anchorage regions.

A practical method is still required to control the crack width of this material. Since the post-cracking behavior of HPFC is different from that of normal strength concrete, the classic tension stiffening model, developed for normal strength concrete, is not directly applicable. In this paper, the conventional tension stiffening theory is extended to fiber reinforced concrete, by taking the post-cracking performance of HPFC into account. Several simplifications with regard to the tensile behavior of HPFC are introduced. The mathematical expressions derived are validated against a number of tensile tests carried out in the Stevin Laboratory at Delft University of Technology.

2 Tension stiffening formulation

Plain concrete is not considered to sustain tension after cracking (except for very small crack widths). However, when it is reinforced by steel rebars, it can still carry tension between the cracks. This effect is denoted with the term 'tension stiffening', reflecting that the stiffness of the whole member is larger than that of the single rebar.

For normal reinforced concrete, mathematical models have been developed and validated by experiments. As referred in [fib MC, 1990] almost 60 formulas have been developed world-widely so far. Despite the simplifications and assumptions in those formulas, the basic differential equations behind them are identical [fib MC, 1999], [Balázs, 1993], [Fehling and Leutbecher, 2007], [Stang and Aarre, 1992] and can be expressed as:

$$\frac{d^2 s}{dx^2} - \frac{1-n\rho}{A_s E_s} \varnothing \pi \tau_b(s) = 0 \tag{1}$$

This equation is in general based on the compatibility condition: $\frac{ds}{dx} = \varepsilon_s - \varepsilon_c$, and the equilibrium condition: $\frac{dF_s}{dx} = \frac{dF_c}{dx} = \tau_b \varnothing \pi$

Moreover the equilibrium of forces in each cross section should be fulfilled:

$$F_s + F_c = N \tag{2}$$

since the stress of the concrete can not exceed the tensile strength f_{ct} the condition

$$\sigma_{cx} < f_{ct} \tag{3}$$

holds true as well.

By setting the origin of the coordinate system in the middle between two cracks spaced

at a distance 2*l* (see Fig. 1), the boundary conditions for plain concrete are:

$$x = 0, \quad s(0) = 0$$

$$x = l, \quad \sigma_{cx} = 0, \sigma_{sx} = \frac{N}{A_s} \text{ and } \frac{ds}{dx} = \frac{N}{A_s E_s} \tag{4}$$

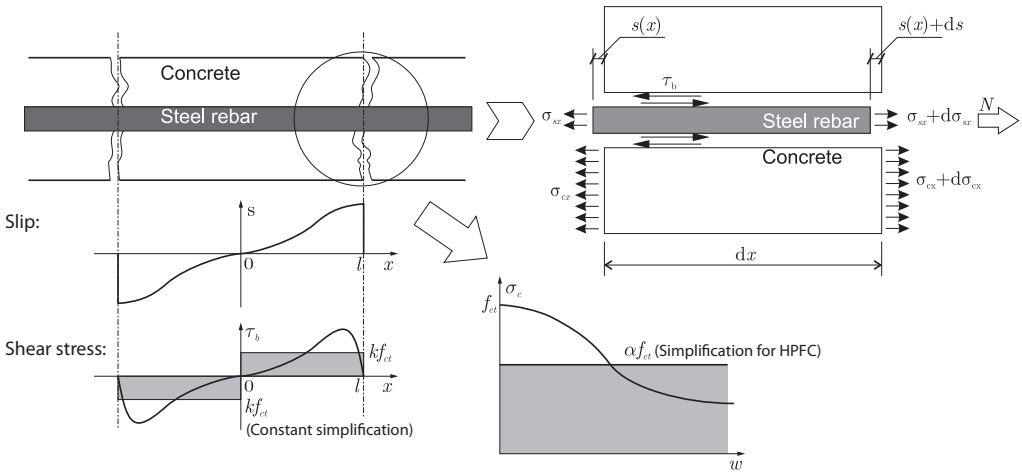

Figure 1: Stress distribution along the length between two cracks

However, as referred to before, as a result of the addition of fibers HPFC is much more ductile than plain cementitious materials, which means that even after cracking, tensile stresses can still be transmitted across the cracks. In order to relate the experimental behavior directly to the stress $\sigma_{c,cr}$ at a crack, this stress can be expressed as a function of the crack opening displacement (COD) *w*, according to $\sigma_{c,cr} = \sigma(w)$. By definition, the crack width *w* is equal to the summation of the slip *s*(*l*) at both sides of the crack.

Thus the boundary condition expressed in equation (4) can be rewritten as:

$$x = l, \quad \frac{ds}{dx} = \frac{N}{A_s E_s} - \sigma_c(w)\left(\frac{A_c}{A_s E_s} - \frac{1}{E_c}\right) \tag{5}$$

The equations listed in this section can be used as general expressions to describe the cracking performance of any type of reinforced composite. With some implementations of material properties such as the shear stress-slip relationship $\tau - s$ and the stress-crack opening relationship $\sigma_c - w$, an expression for the slip distribution $s(x)$ along the bar can be derived. Furthermore, the development of the steel stress and the bond stress along the length of the reinforced element can be described.

3 Derivation of a simplified model

As mentioned before, because of differences in fiber type, fiber content, test methods and other influencing factors, the constitutive relations of HPFC can deviate substantially from each other. For those types of HPFC which exhibit strain hardening after first cracking, densely distributed cracks will occur before the peak stress is reached. This is defined as multiple cracking. In the strain hardening stage, the deformations of concrete and steel rebar are still compatible. Thus there is no slip between concrete and steel rebar in that stage [Fischer, 2002]. The cracks in this situation can be explained with the so called ACK model developed in [Aveston et al., 1971] at the meso level, which is not within the scope of this paper. In this study, the deformation of HPFC in the strain hardening phase is simplified as equivalent strain. It is proven that for steel fiber reinforced concrete (SFRC), by increasing the amount of steel fibers, this strain hardening effect can be maintained until a relatively high stress level, such as shown by concretes like Ductal, which can reach a bending tensile strength of 50 MPa according to [Acker and Behloul, 2004]. However, in many cases the use of steel fibres only is not economic. By combining steel fibers with reinforcement, more economic composite is obtained. Therefore, in this paper the softening behavior of HPFC is of more interest. The bond between concrete and steel rebar is only activated after the peak stress of the concrete has been reached. By employing differential equation (1), together with a proper description of the post-cracking performance of HPFC in equation (5), it is possible to predict the composite behavior of reinforced HPFC.

For the post cracking performance of HPFC, different models can be found in literature, such as: the exponential model [Stang and Aarre, 1992], [Redaelli and Muttoni, 2007] $\sigma(w) = f_t / (1 + (w/w_0)^p)$, the bilinear model [Schumacher, 2006] $\sigma(w) = a_i + b_i w$, the constant model [Bischoff, 2003] $\sigma(w) = \alpha f_{ct}$, and others [Fehling and Leutbecher, 2007].

In general the advantage of a more complex constitutive model is that with those models, the experimentally observed cracking performance can be described more precisely, whereas the drawback is that a sophisticated numerical iteration is required to make use of these models, which costs time and requires more information from experimental results. Obviously, most of the models are too complicated for engineering application. Therefore in this paper, in order to get a simplified relationship between cracking and stress in a HPFC element, a constant tensile stress level after cracking is adopted:

$$\sigma(w) = \alpha f_{ct} \tag{6}$$

where α is a reduction factor that is related to the steel fiber content, the tensile strength of the cementitious matrix, and the loading condition. The value of α can be derived from tests, such as the direct tensile test.

On the other hand, in order to solve the differential equation, a proper bond-slip relationship ($\tau - s$) is necessary. Many efforts have been made to describe the bonding stress between concrete and steel rebars since the 1960s [Braam, 1990], with the aim to formulate the composite behavior of normal reinforced concrete. Various expressions have been developed for that purpose. Some are: the exponential relation [Balázs, 1993], [Fehling and Leutbecher, 2007]: $\tau_b = \tau_{\max} (s/s_1)^{\beta}$, and the linear relation [Fehling and König, 1988]: $\tau_b = a_1 + a_2 s$.

However, as was reported in [Fehling and König, 1988], a constant value of the bond stress already offers enough accuracy in predicting the test results, when it is related to the mean tensile strength of the concrete. Based on a similar simplification principle as with the post-cracking stress, the bond stress of HPFC is expressed as a constant value, which is directly related to the concrete tensile strength:

$$\tau_b = k f_{ct} \tag{7}$$

The value of k should be based on experimental results: as a first estimation, the value $k = 2$ is used. Once this bond stress distribution $\tau_b(s)$ is known, the stress in the concrete at the origin σ_{c0} can be formulated based on the value of $\sigma_c(w)$ at the crack:

$$\sigma_{c0} = \int_l^0 \frac{\tau_b(s) \varnothing \pi}{A_c} dx + \sigma_c(w) \tag{8}$$

Thus, the transmission length l_t, which is required to develop another crack in HPFC is then expressed, according to (3) and (8), as:

$$l_t = \frac{f_{ct}(1-\alpha)\varnothing}{4\tau_b \rho} \tag{9}$$

4 Solution

With given boundary conditions, the differential equation (1) can be solved analytically, for which the value of l in the boundary condition (5) is set to be l_t.

By substituting the expression of σ_c (w) (6) into the boundary conditions, the differential equation (1) is solved analytically. The expression for $s(x)$ becomes:

$$s(x) = \frac{2kf_{ct}}{\text{Ø}E_s}(1 - n\rho)x^2 + Cx \tag{10}$$

with

$$C = \frac{N}{A_s E_s} - \frac{f_{ct}}{E_s \rho}(1 - n\rho)$$

Furthermore, the maximum crack opening in the HPFC element can be estimated by checking the value of $s(l_t)$. The maximum crack opening after crack formation has stabilized can then be expressed as:

$$w_{\max} = \frac{f_{ct}(1-\alpha)\text{Ø}}{4\tau_b \rho E_s}\left(\frac{N}{A_s} - \frac{f_{ct}}{2\rho}(1 - n\rho)(1+\alpha)\right) \tag{11}$$

Based on the simplification given above, a simple analytical model is obtained, with two constants related to the HPFC material behavior: the strength reduction factor α and the bond strength factor k. The tension stiffening effect in a reinforced HPFC element can be simulated analytically with this model. A schematic load displacement relationship according to this model is plotted in Fig. 2, in which one can find that the response of a reinforced HPFC element can be subdivided into five stages. These are: the linear elastic stage, the hardening (multiple cracking) stage, the (macro-) crack formation stage, the stabilized cracking stage and the yielding stage of the steel rebar. The transition between the stages is characterized in Fig. 2 by the points O, A, B, and C. Since the effect of multiple cracking of HPFC is treated as uniformly distributed strain, the first macro-crack is supposed to occur when the HPFC reaches its maximum tensile strength.

After the crack pattern has been stabilized the difference between HPFC and normal concrete can be observed. In this stage there are two mechanisms for the concrete to

transmit the tensile stresses along the element, see Fig. 2, namely the bond between concrete and steel rebar, which is similar to that of normal reinforced concrete, and the post-cracking strength αf_{ct} . The former one vanishes after yielding of the rebar, whereas the post-cracking stress transmitted across the cracks, provided by the fibres, is still active, even after yielding of the reinforcing steel. Both mechanisms enable that the element carries a larger load than a naked rebar, even after the HPFC element has been cracked.

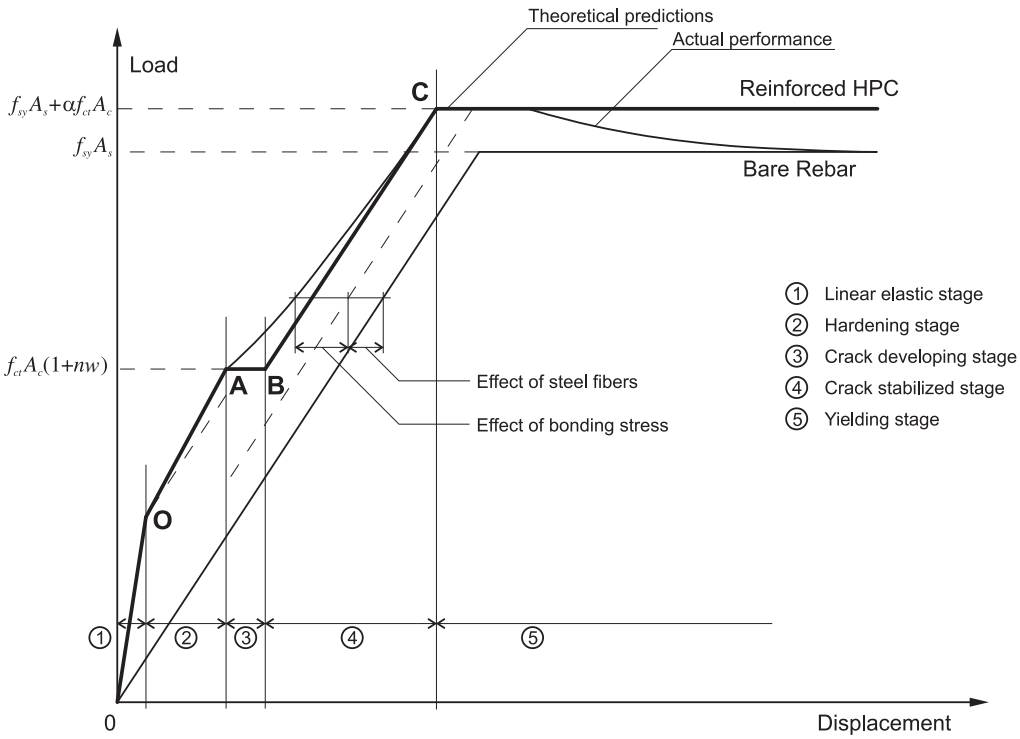

Figure 2: Schematic load-displacement relationship for a reinforced HPFC prismatic bar loaded in tension

It is assumed that in the stabilized cracking stage the mean crack distance is $1.5l_t$. From the position of a crack to the middle between two cracks, the stress of the steel rebar σ_s reduces by:

$$\Delta\sigma_s = 0.75\frac{f_{ct}(1-\alpha)}{\rho} \tag{12}$$

Thus the average strain of the steel rebar ε_{sm} is equal to $(2\sigma_s - \Delta\sigma_s)/2E_s$. Since the average strain of the whole member is equivalent to that of the steel rebar, the average strain of the member is:

$$\varepsilon_{sm} = \frac{1}{E_s}\left(\sigma_s - 0.375\frac{f_{ct}(1-\alpha)}{\rho}\right)$$

Due to the high percentage of cement in the concrete mixture, the shrinkage deformation of HPFC should not be neglected, when calculating the mean strain of the reinforced element. For a high strength concrete with a compression strength around 100 MPa, the strain due to autogenous shrinkage and drying shrinkage is about 0.4‰ (after 28 days) according to Eurocode 2. This value is used in this study when analyzing the results of the tensile tests.

Summarizing, an analytical solution has been given to describe the tension stiffening effect of a reinforced HPFC element. In order to solve the differential equation, so that an easily applicable solution can be derived, it is assumed that the bond stress and the tensile stress transmitted across the cracks is constant, independent of the bar slip and the crack opening. These assumptions have to be validated on the basis of experimental results.

5 Experimental study

Tests have been carried out at Delft University of Technology [Shionaga et al., 2006] in order to quantify the combined effect of reinforcement and steel fibers in a reinforced HPFC member. The tests on a concentrically reinforced member are introduced here briefly in order to validate the simplified model developed in this paper. The configuration of the tests is shown in Fig. 3. More information can be found in [Shionaga et al., 2006].

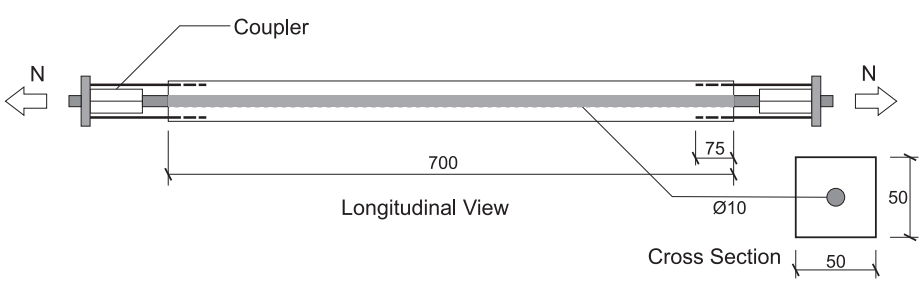

Figure 3: Configuration of direct tensile test on a concentrically reinforced concrete prism

The concrete prismatic members were concentrically reinforced by a ribbed rebar with yield strength of 530 MPa. The Young's modulus of the rebar is 190 GPa according to a control tensile test and the diameter of the bar is 10 mm. Five series of axial tensile tests were carried out in which fiber type and contents were varied. The fiber contents were 0, 0.8 and 1.6 vol%. For the HPFC with 1.6 vol% fibers, the fiber aspect ratio was 37.5, 66.7 and 81.3, respectively. For each series, three specimens were tested and the mean results were used for further analysis. The main parameters of the test series are listed in Table 1.

Table 1: Parameters of test series

Variables	Notation	No.1	No.2	No.3	No.4	No.5
Concrete strength class	f_c' [MPa]	B130	B130	B130	B130	B130
Fiber content	V_f [vol%]	0	0.8	1.6	1.6	1.6
Fiber type	$L_f\,d_f$ [mm]	-	13 ·0.16	13 ·0.16	20 ·0.3	6 ·0.16
Aspect ratio	L_f / d_f [-]	-	81.3	81.3	66.7	37.5

In order to avoid disturbance of the fiber orientation by the mould, the specimens of the same series were cast together as a plate. After 28 days, when the strength of the concrete matrix had reached the target strength, the plates were sawn into prismatic specimens with the required dimensions. The compressive strength of the 100 mm HPFC cubes was about 130 MPa at the age of 28 days, which did not change substantially as a function of the fiber content. On the contrary, as predicted before, the tensile behavior of the HPFC was highly dependent on its fiber content. Therefore, a number of direct tensile tests were carried out additionally in order to determine the reduction factor α.

6 Post-cracking behavior of HPFC

In this study the post-cracking behavior of HPFC was tested with a dog-bone shaped specimen subjected to direct tensile loading. Only steel fibers with an aspect ratio of 81.3 were used in those tests. The content of the fibers in each test series was the same as mentioned before. For every series, the average behavior was determined on the basis of four tests. The dimensions of the dog bone specimens are as shown in Fig. 4. As indicated there, the minimum cross section of the specimen was 70 · 70 mm. Before carrying out the tensile test, the specimens were cured during 28 days, and their two ends were cut-off in order to eliminate the influence of the mould.

Two sets of tests results for each test series are plotted in Fig. 5. As explained before, the results of the tensile tests strongly depend on the fiber content of the HPFC. Fig. 5 shows that, with regard to plain concrete, 0.8 vol% of steel fibers does not lead to a substantial increase of the tensile strength of the concrete, but the ductility of the mixture is clearly improved. However, if the fiber content is further increased to 1.6 vol%, the rise of the tensile strength of the mixture is obvious. Thus, it can be concluded that the peak strength of the HPFC is determined by both the tensile strength of the matrix and the fiber content. Based on that conclusion, the following formula is used in this paper to predict the tensile strength of HPFC [Fischer, 2004]:

$$f_{ct} = k_1 f_{mt} + k_2 V_f \frac{l_f}{d_f} \tag{14}$$

where

k_1 and k_2 are factors which should be determined by experiments.

f_{mt} is the tensile strength of plain concrete.

Further to the significant influence of the fiber content on the peak load of HPFC, even for the same content, the results in Fig. 5 demonstrate that there is some scatter.Depending on the position of crack localization, a hardening path may occur before the peak stress is reached. On the other hand, after the peak stress has been passed, the stress-strain relations obtained do not vary much. Since the post cracking stress is not constant an

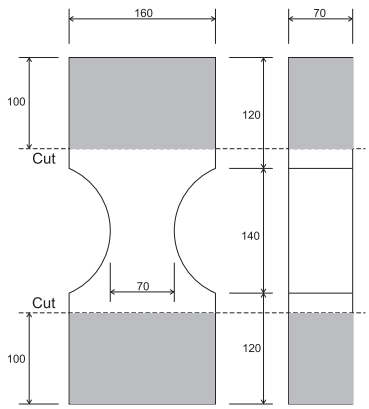

Figure 4: Configuration of the dog bone specimens

appropriate choice for the post-cracking stress has to be made. Here, conservatively, the stress level αf_{ct} is chosen to comply with the crack opening of 0.8 mm. According to equation (11), the reinforcement has already started yielding before the maximum crack width has reached this value. Therefore, the value of α is set as 0.8 before further analysis is carried out. It should however, already in advance be noted that the fiber orientation in the dog-bone specimen and the tensile behavior may not be the same. A possible reconsideration of the value 0.8 may therefore be necessary when further evaluating the results.

In Fig. 6, the peak stress of the HPFC specimens is plotted against the fiber content, and the values of k_1 and k_2 are determined by curve fitting (k_1 = 0.9 and k_2 = 0.04). Thus, the strength of HPFC with different fiber contents can be estimated and applied in predicting the tension stiffening effect.

7 Test results

In order to evaluate the influence of the post-cracking strength on the tension stiffening effect, the mean tensile responses of the specimens with fiber contents of 0, 0.8 and 1.6 vol% are plotted together in Fig. 7. The results demonstrate that the plain concrete barely contributes to the stiffness of the member, which is not in agreement with the expected behavior as explained in section 2. A possible explanation is that before the external load is

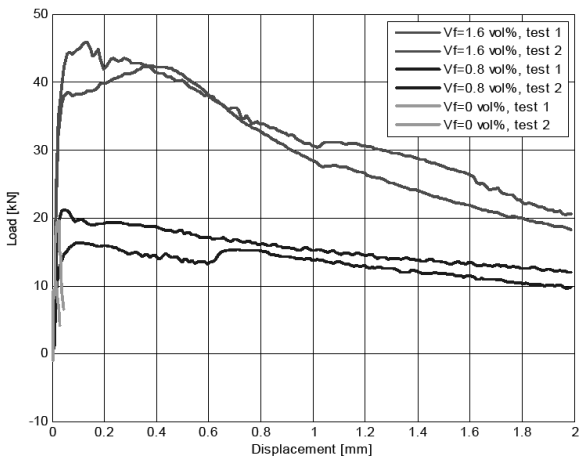

Figure 5: Result of dog-bone tensile tests

applied to the reinforced element, tensile stresses have developed due to shrinkage of the concrete. As was explained before, according to Eurocode 2, the high water/binder ratio used in the mixtures can result in a shrinkage strain of about 0.4‰ unless the concrete is restrained by the rebar. Apparently this influence of shrinkage shall be taken into account. Therefore the curves of all the test results are adjusted by the shrinkage deformation before they are analyzed.

As indicated in Fig. 2, the tensile performance of the concentrically reinforced HPFC

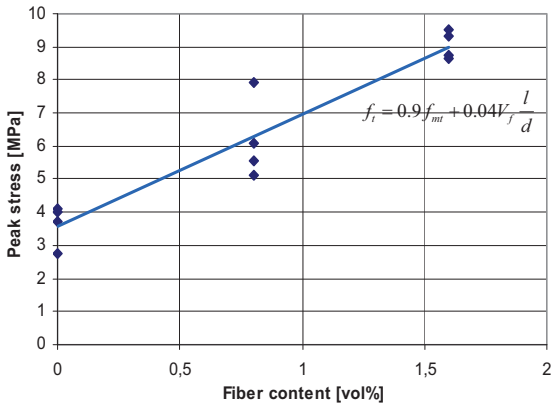

Figure 6: Relationship between fiber content and peak stress

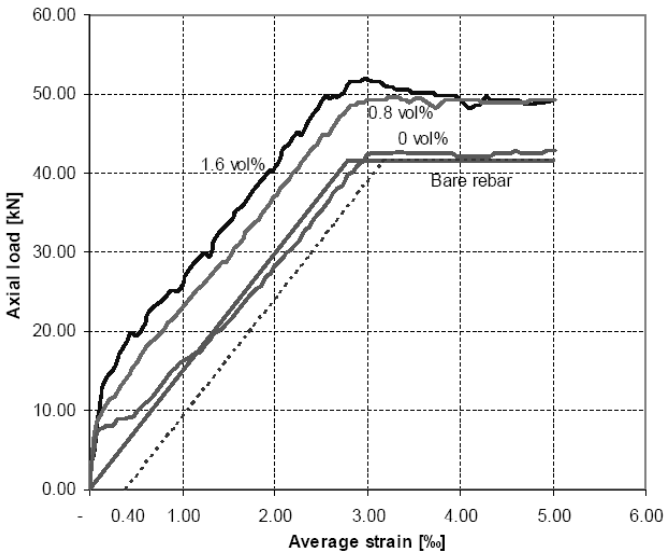

Figure 7: Response of reinforced specimens under direct tension

element can be subdivided into several stages. Because of the simplifications given before, in any stage the load-displacement relationship of the specimen is linear. If strain hardening of the concrete is not considered, four sections remain from the load-displacement curve shown in Fig. 2. To describe them analytically, the expressions for the points A, B, and C in Fig. 2 are essential. Based on Equation (9) and (13) developed in Sect. 4, they can be formulated as:

Point A (end of the elastic stage):

$$\varepsilon_A = \frac{f_{ct}}{E_c}, \quad F_A = f_{ct} A_c (1 + n\rho). \tag{15}$$

Point B (end of the crack formation stage):

$$\varepsilon_B = \varepsilon_A + 0.625(1-\alpha)\frac{f_{ct}}{\rho E_s}, \quad F_B = F_A. \tag{16}$$

Point C (yielding of steel rebar):

$$\varepsilon_C = \frac{1}{E_s}\left(f_y - 0.375\frac{f_{ct}(1-\alpha)}{\rho}\right), \quad F_C = f_y A_s + \alpha f_{ct} A_c. \tag{17}$$

Those values shall be further adjusted by the influence of the initial shrinkage. If the shrinkage strain of HPFC is ε_{sh} without rebar, the initial strain and the corresponding restraining force in the reinforced member become:

$$\varepsilon_{sh0} = \frac{\varepsilon_{sh} n\rho}{1 + n\rho}, \quad F_{sh0} = A_s E_s \varepsilon_{sh0}. \tag{18}$$

Based on the given expressions, the test results are compared with the analytical prediction in Fig. 8 and Fig. 9. Both figures show that it is possible to predict the tension stiffening effect of a concentrically reinforced HPFC element reasonably well with this simplified method.

Fig. 8 shows that, after the rebar starts to yield, the model becomes less accurate. This has to do with the fact that after the steel yields the deformation of the whole member localizes in a limited number of cracks. After localization the crack opening increases dramatically. In that situation, the stress-crack opening relationship of a single crack in HPFC becomes dominant in the overall behavior of the whole member. This conclusion can be further confirmed by the crack pattern of the reinforced HPFC element as plotted in Fig. 10, where the deformations of the composite elements are highly localized after yielding of the

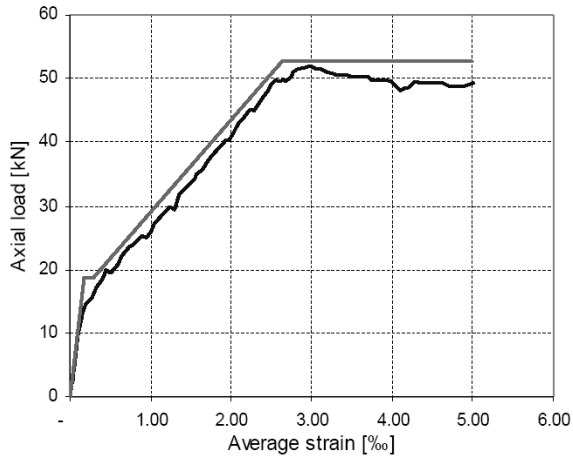

Figure 8: Comparison between test result and model prediction (V_f = 1.6 vol%)

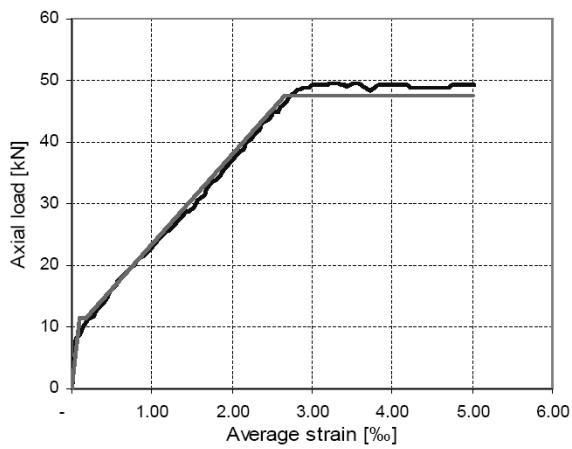

Figure 9: Comparison between test result and model prediction (V_f = 0.8 vol%)

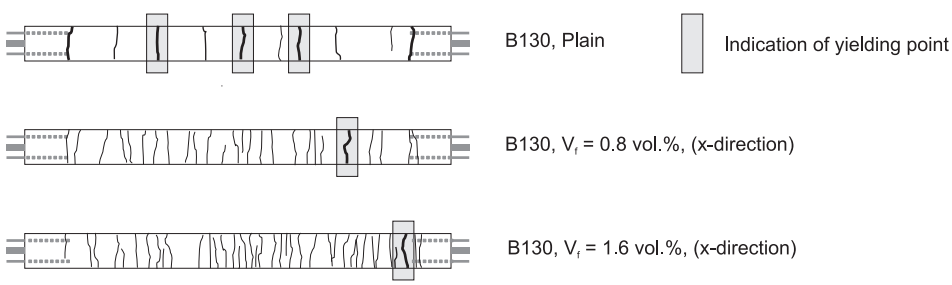

Figure 10: Crack distribution of the specimen after yielding

rebars. With increasing fiber content, localization is more likely to occur in one crack, because of the scatter in fiber content along the specimen.

The average crack spacing of the concrete member is calculated from Fig. 10 by dividing the effective length of the specimen by the number of cracks. The results are given in Table. 2. According to Eq. (9), the crack spacing can be predicted if the value of α is known. With the assumed value $\alpha = 0.8$, as obtained from the dog bone test, the transmission length l_t is calculated. Furthermore, with regard to the assumption that the average crack spacing l_{cr} is about $1.5l_t$, it is found that the mean crack spacing is 11.56 mm for both fiber concretes. Since the value of friction stress τ_b is determined by the tensile strength of the HPFC, the average crack spacing does not change in this case. This shall be further validated by experiments. And in general the prediction is lower than observed in the tests. A possible reason is that either the value of α or τ_b is not accurate enough. As already stated before, this can be due to differences in fiber orientation between the dogbone test and the centric tensile test on the reinforced prismatic member. Therefore α is determined in another way. To this aim, the concrete contribution of the overall capacity is derived from Fig. 8 and Fig. 9. The resulting post-cracking tensile stress is plotted in Fig. 11 as a function of the strain. In a similar way as before, the initial autogenous shrinkage as well as drying shrinkage of the concrete member is taken in to account.

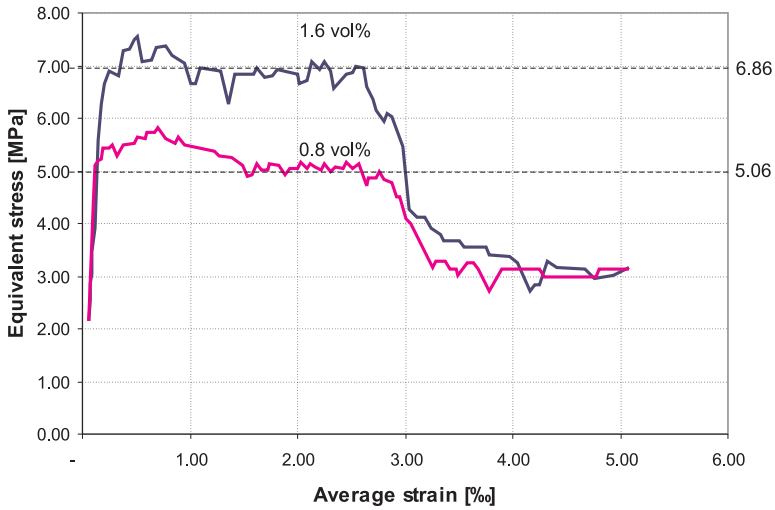

Figure 11: Load contribution of the concrete in the tensile member as derived from Fig. 8 and 9

Table 2: Crack distribution along the specimen

Strength class	V_f [vol.%]	Average crack spacing	Number of cracks
B130	0	56.0	11
	0.8-x	22.7	25
	1.6-x	14.2	40

Contrary to the results from the direct (dog bone) tensile test, a yielding plateau is found after the crack pattern has been stabilized along the prism. As explained before, this is because of the confinement of the crack width due to the existence of the steel rebar. In Fig. 11 the average stress level of the two concretes, with different fiber content, is shown. With regard to the average crack spacing length $1.5l_t$, the average stress of the concrete member can be expressed with

$$\sigma_c = f_{ct}\left(\frac{3}{8}+\frac{5}{8}\alpha\right).$$

Thus the actual values of α for fiber contents of 1.6 vol% and 0.8 vol% are determined for the given concrete strength f_{ct} . By introducing an average value of α = 0.68 into equation (9), the mean crack spacing becomes l_{cr} = 18.5 mm for both fiber contents. This corresponds reasonably well with the crack spacings observed in the tests, which are 22.7 mm for 0.8 Vol.% fibres and 14.2 mm for 1.6 Vol.% fibres respectively. Regarding the

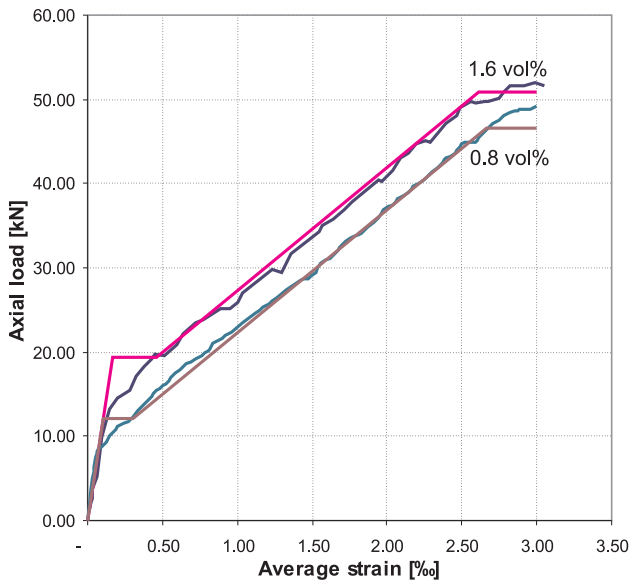

Figure 12: Comparison between test result and model prediction after adjustment of α

scatter due to differences in fiber orientation this value already provides a quite reasonable prediction. Subsequently the new α value is used in order to adjust the overall behavior of the element. As confirmed by Fig.12 a better agreement is achieved, especially in the stabilized stage.

8 Conclusion

In this paper, the combined effect of High Performance Fiber Concrete and steel rebar is formulated based on an extension of the tension stiffening theory for normal (plain) concrete. To solve the differential equations, a simplified assumption is proposed, which implies that the tensile stress of HPFC is constant in the post-cracking stage. A strength reduction factor α is introduced according to this assumption. By solving the equations, the crack width before yielding and the tensile performance of the reinforced HPFC element are analytically expressed.

A number of reinforced prismatic elements with different fiber contents were tested at Delft University of Technology. The test results were used to evaluate the simplified method presented in this paper. After adjustment for the initial shrinkage deformation of the HPFC, this simplified model predicts the test results within a reasonably range. Thus it can be concluded that before the steel reinforcement yields, it is possible to assign a constant post-cracking strength as well as a constant bond strength. However, the value of this post cracking strength αf_{ct} shall be evaluated in an appropriate way. To achieve this, a new test or assessment method should be developed based on a better understanding of the post cracking performance of HPFC, reinforced by steel rebars. Furthermore, a careful check on the influence of steel fibers on the bond between rebar and concrete shall be done.

Notation

F_s : force in steel rebar

F_c : force in concrete

N : total force

Ø : diameter of rebar

$s(x)$: slip between concrete and steel rebar, it is a function of position x

ε_{sx} : strain in steel rebar at position x

ε_{cx} : strain in concrete at position x

ε_{sh} : initial strain due to shrinkage of HPFC

τ_b (s) : bond between concrete and steel, it is a function of slip s

τ_{bx} : bond stress at position x

σ_{sx} : stress in steel rebar at position x

σ_{cx} : stress in concrete at position x

A_s : area of the steel rebar

A_c : area of concrete

α : strength reduction factor

k : factor for bond stress on concrete-steel interface

n : ratio of elastic moduli of steel and concrete, $n = E_s / E_c$

ρ : ratio of areas of steel and concrete, $\rho = A_s / A_c$

w : crack width

l_t : transmission length

l_{cr} : average crack spacing

l_f : length of fibers

d_f : diameter of fibers

ε_{sm} : average strain of the steel rebar

$\sigma_{s,cr}$: stress of steel rebar at cracks

$\sigma_{c,cr}$: stress of concrete through cracks, it is a function of crack width σ_c (w)

$\Delta\sigma_s$: stress range in the steel rebar with average crack distance

f_{ct} : tensile strength of HPFC

f_{mt} : tensile strength of plain concrete matrix in HPFC

k_1 and k_2 : influencing factors of HPFC strength based on experimental results

V_f : fiber content in HPFC

Literature

Acker, P. and M. Behloul, "Ductal Technology: a large spectrum of properties, a wide range of applications", *International symposium on ultra high performance concrete*, 2004, Kassel University Press, Kassel.

Aveston, J., G.A. Cooper, and A. Kelly, "Single and multiple fracture", *The properties of fibre composites*, 1971, National Physical Laboratory.

Balázs G. L., "Cracking analysis based on slip and bond stresses", *ACI materials journal*, 1993, 90 (37), pp. 340-348.

Bischoff, P.H., "Tension stiffening and cracking of steel fiber-reinforced concrete", *Journal of materials in civil engineering*, 2003. 2 (15): pp. 174-182.

Braam, C.R., "Control of crack width in deep reinforced concrete beams", *Heron*, 1990, 35 (4): pp. 3-105.

Fehling, E. and G. König, "Zur Rissbreitenbeschränkung im Stauhlbetonbau", *Beton- und Stahlbetonbau*, Vol. 83, Nos. 6/7, 1988, pp. 161-167, 199-204.

Fehling, E. and T. Leutbecher, "Tensile behavior of ultra high performance concrete (UHPFC) reinforced with a combination of steel-fibers and rebars", *3rd international conference on structural mechanics and computations*, 2007, Cape Town.

FIB Model Code 1990, fib bulletins 2: Structural Concrete, 1999.

Fischer, G. and V.C. Li, "Influence of matrix ductility on tensile-stiffening behavior of steel reinforced engineered cementitious composites (ECC)", *ACI structural journal*, 2002 (99-S12): pp. 104-111.

Fischer, G. "Current U.S. guidelines on fiber reinforced concrete and implementation in structural design", *Fiber reinforced concrete from theory to practice*, 2004, Bergamo, Italy.

Redaelli, D. and A. Muttoni, "Tensile behaviour of reinforced ultra-high performance fiber reinforced concrete element", *fib Symposium: Concrete structures: stimulators of development*, 2007, Dubrovnik, Croatia.

Schumacher, P., "*Rotation Capacity of Self-Compacting Steel Fiber Reinforced Concrete*", 2006, PhD thesis, Darmstadt University of Technology, Darmstadt.

Shionaga, R., et al., "Combined effect of steel fibers and steel reinforcing bars in High Performance Fiber Reinforced Concrete", *In HB Fischer (Ed.), Ibausil, 16th. internationale Baustofftagung*, 2006, Bauhaus Universitat, Weimar, Germany.

Stang, H. and T. Aarre, "Evaluation of crack width in FRC with conventional reinforcement", *Cement & Concrete Composites*, 1992, 14, pp. 143-154.

Li, V.C., "On Engineered Cementitious Composites (ECC): A Review of the Material and Its Applications", *Journal of Advanced Concrete Technology*, 2003, pp. 215-230.